Shear reduction of collisional transport: Experiments and theory[a)]

C. F. Driscoll,[b)] F. Anderegg, D. H. E. Dubin, D.-Z. Jin,[c)]
J. M. Kriesel,[d)] E. M. Hollmann,[e)] and T. M. O'Neil
Physics Department and Institute for Pure and Applied Physical Sciences, University of California at San Diego, La Jolla, California 92093-0319

(Received 1 November 2001; accepted 26 December 2001)

Experiments and theory on collisional diffusion and viscosity in quiescent single-species plasmas demonstrate enhanced transport in the two-dimensional (2D) bounce-averaged regime, limited by shear in the plasma rotation. For long plasma columns, the measured diffusion agrees quantitatively with recent theories of three-dimensional long-range $\mathbf{E}\times\mathbf{B}$ drift collisions, and is substantially larger than predicted for classical velocity-scattering collisions. For short plasmas, diffusion is observed to be enhanced by N_b, the number of times a thermal particle bounces axially before being separated by shear. Equivalently, recent theory in the 2D bounce-averaged regime shows how diffusion decreases with increasing shear, generalizing the zero-shear perspective which gives Bohm diffusion. Viscosity is similarly enhanced in the 2D regime, but there is presently only qualitative agreement with theory. These results apply to both non-neutral and neutral plasmas, and provide the first rigorous analysis of shear reduction of transport in a paradigmatic system. © *2002 American Institute of Physics.* [DOI: 10.1063/1.1454998]

I. INTRODUCTION

In the classical theory of collisional transport,[1–4] the transport step is caused by velocity-scattering collisions, as shown in Fig. 1(a). The local binary collision produces scattering of the particle velocity vectors by $\Delta v \approx \pm \overline{v}$, which results in cross-field step of the guiding centers by a distance $\Delta r \approx \pm r_c$. These ''short-range'' collisions occur only for impact parameters ρ in the range $\rho \lesssim r_c$.

However, the Coulomb interaction between particles extends to (at least) a distance λ_D; and when $r_c \ll \lambda_D$, most collisions have impact parameters in the range $r_c < \rho < \lambda_D$. These collisions are neglected in classical transport theory, and are only now being quantitatively analyzed. The basic transport steps of these ''long-range'' collisions are shown in Fig. 1(b); as two particles separated by a distance ρ in θ stream by each other along $B\hat{z}$, they $\mathbf{E}\times\mathbf{B}$ drift a distance $\pm\Delta r$ due to their mutual interaction field ΔE. The step Δr is proportional to the duration Δt of the interaction, so ''resonant'' pairs of particles with small relative axial velocity Δv_z will take the largest steps Δr.

These three-dimensional (3D) long-range collisions give substantially different transport coefficients for particle diffusion,[5–8] shear viscosity,[6,9,10] and heat conduction,[11–13] as shown in Table I. The classical transport arises from random steps of size r_c occurring at a collision rate $\nu_c \equiv n\overline{v}b^2$, so the transport coefficients scale as $\nu_c r_c^2$. In contrast, the long-range interaction distance of λ_D introduces the possibility of coefficients scaling as $\nu_c \lambda_D^2$. This latter scaling is obtained for viscosity and heat transport; but the 3D long-range diffusion has the same $\nu_c r_c^2$ scaling as classical transport, with a $10\times$ larger coefficient.

Moreover, the diffusion[14] and viscosity[15,16] due to long-range collisions is enhanced in the two-dimensional (2D) regime, where individual particles in the finite length plasma bounce repeatedly in z before moving substantially in (r,θ). From the perspective of Fig. 1(b), this suggests that pairs of particles may experience multiple correlated collisions, giving an enhanced transport step size Δr. This enhancement increases with N_b, the number of times a thermal particle bounces axially before shear in the θ rotation of the column separates the particle from its neighbors. Thus, rotational shear reduces the 2D transport enhancement.

In practice, the transport contributions from long-range collisions and the 2D enhancements described here are not subtle. The test particle diffusion measured on pure ion plasmas is $10-10^3$ times larger than classical theory; thermal transport in ion plasmas is 1–200 times larger; and the viscous transport measured in pure electron plasmas is $10-10^8$ times larger. In general, these results are in substantial agreement with new theories of collisional transport; the largest discrepancy is in the viscosity coefficient, where finite-length enhancements give a one-decade discrepancy with theory.

The transport observed in non-neutral plasmas is large compared to classical theory because these plasmas are necessarily in the guiding-center regime of $r_c < \lambda_D$. The classical theory, developed for neutral plasmas, implicitly assumes the opposite ordering of $r_c \gg \lambda_D$, although not all neutral plasmas are in this regime either.

For completeness, we note that particles can exchange energy and momentum over distances up to the plasma size R_p by emission and absorption of lightly damped plasma

[a)]Paper BI2 2, Bull. Am. Phys. Soc. **46**, 22 (2001).
[b)]Invited speaker.
[c)]Present address: Department of Brain and Cognitive Sciences, MIT, Cambridge, MA 02139.
[d)]Present address: Natl. Inst. of Standards and Technology, 325 Broadway, Boulder, CO 80309.
[e)]Present address: Center for Energy Research, University of California at San Diego, La Jolla, CA 92093-0417.

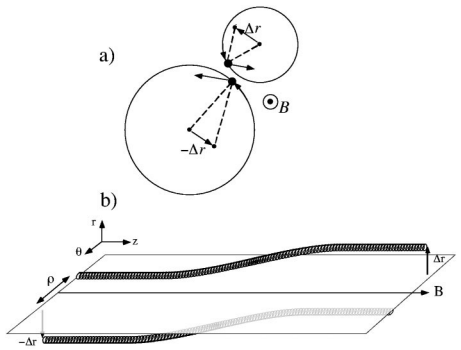

FIG. 1. (a) Classical velocity-scattering collisions with impact parameters $\rho \lesssim r_c$. (b) Long-range **E×B** drift collisions with $r_c < \rho < \lambda_D$.

waves. This wave mechanism was originally proposed by Rosenbluth and Liu[11] as a possible explanation of the anomalously large heat loss through the electron channel in tokamak plasmas, and has been recently developed further by Ware.[17] Recent calculations suggest[12] that this mechanism will dominate the viscosity for non-neutral plasmas with $R_p > 10^3 \lambda_D$, and dominate the heat transport for $R_p > 10^2 \lambda_D$. However, experiments have not yet been done in this regime.

The transport being discussed here is due to the thermal fluctuations which occur even in quiescent (near thermal equilibrium) plasmas at any given temperature T. The fluctuations can be large at high temperatures; but the spectrum remains thermal, and statistical theory determines the transport explicitly. In contrast, turbulent plasmas can have an extremely nonthermal spectrum of fluctuations, with the transport characteristics depending on the nature of the turbulence. However, the effects of flow shear may be similar in both cases, and the present work may be considered a simple paradigm for the shear reduction of transport seen in more complex turbulent systems.[18]

II. TEST PARTICLE DIFFUSION (3D REGIME)

The radial diffusion of "tagged" ions has been measured in quiescent, steady-state columns of Mg^+ ions.[8] These pure ion plasmas are contained in vacuum ($P \approx 3 \times 10^{-9}$ Torr) in cylindrical electrodes with wall radius $R_w = 2.86$ cm, as shown in Fig. 2. A uniform axial magnetic field ($0.8 < B (0.8 < B < 4$ T) provides radial confinement; and voltages $V_c = +200$ V applied to end cylinders provide axial confinement of the ions.

The ion plasma is diagnosed by laser-induced fluorescence (LIF), stimulated by tuneable continuous wave laser beams in the parallel ($\hat{z}$) or perpendicular ($\hat{y}$) directions. These beams can be scanned in x, and the intersection with the detection focus along the x axis determines a 1 mm^3 diagnosed volume. The LIF diagnostic gives ion density $n(x) = n(r)$, temperature $T(r)$, and total drift velocity in the $\hat{y} = \hat{\theta}$ direction, denoted $v_{tot}(r)$. Additionally, all particles at a given radius can be "tagged" by spin alignment; and the density $n_t(r)$ of these (dynamically unaltered) test particles can be measured versus time.

Figure 3(a) shows typical measured profiles of $n(r)$ and

TABLE I. Diffusion, viscosity, and heat conduction coefficients due to classical velocity scatterings with impact parameters $\rho < r_c$; and due to long-range **E×B** collisions with $r_c < \rho < \lambda_D$ in the 3D and 2D bounce-averaged regimes.

$\nu_c \equiv n \bar{v} b^2$	Diffusion D	Viscosity η / nm	Heat $2K/5n$
$\rho < r_c$ classical velocity scattering	$\frac{4\sqrt{\pi}}{3} \nu_c r_c^2 \ln(\frac{r_c}{b})$ Longmire & Rosenbluth '56	$\frac{2\sqrt{\pi}}{5} \nu_c r_c^2 \ln(\frac{r_c}{b})$ Longmire & Rosenbluth '56 Simon '55	$\frac{16}{15}\sqrt{\pi} \nu_c r_c^2 \ln(\frac{r_c}{b})$ Rosenbluth & Kaufman '58
$\rho > r_c$ 3D v_z resonance	$2\alpha\sqrt{\pi}\, \nu_c r_c^2 \ln(\frac{\bar{v}}{\Delta v_m}) \ln(\frac{\lambda_D}{r_c})$ (Lifshitz & Pitaevskii) O'Neil '85 Dubin '97 Anderegg '97	$.59\alpha\, \nu_c \lambda_D^2 \ln(\frac{\bar{v}}{\Delta v_m})$ (+ wave) O'Neil '85 Dubin '88 Driscoll '88	$.48 \nu_c \lambda_D^2$ (+ wave) (Rosenbluth & Liu '76) Dubin & O'Neil '97 Hollmann '00
2D z-averaged	$8\pi^2 \frac{f_b}{r\lvert\omega_E'\rvert} \nu_c r_c^2 \ln(\frac{r}{d})$ Dubin & Jin '01 Anderegg '02	$16\pi^2 \frac{f_b}{r\omega_E'} \nu_c d^2 g(2d/r)$ Dubin & O'Neil '98 Kriesel '01	NA

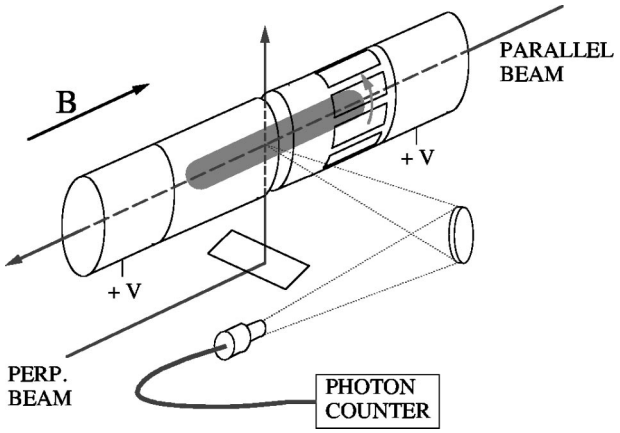

FIG. 2. Ion plasma containment apparatus, with perpendicular and parallel laser beam diagnostics.

$T(r)$. The column has density $n \approx 10^7$ cm^{-3} over a radius $R_p \approx 0.5$ cm and length $L_p \approx 10$ cm. The temperature of $T \approx 0.1$ eV gives an ion thermal velocity $\overline{v} \approx 6.3 \times 10^4$ cm/s, and an axial bounce rate of $f_b(r) \equiv \overline{v}/2L_p \approx 3$ kHz. The scale lengths for short- and long-range collisions are $r_c = 1.6 \times 10^{-2}$ cm (at $B = 1T$) and $\lambda_D = 7.4 \times 10^{-2}$ cm. The ion

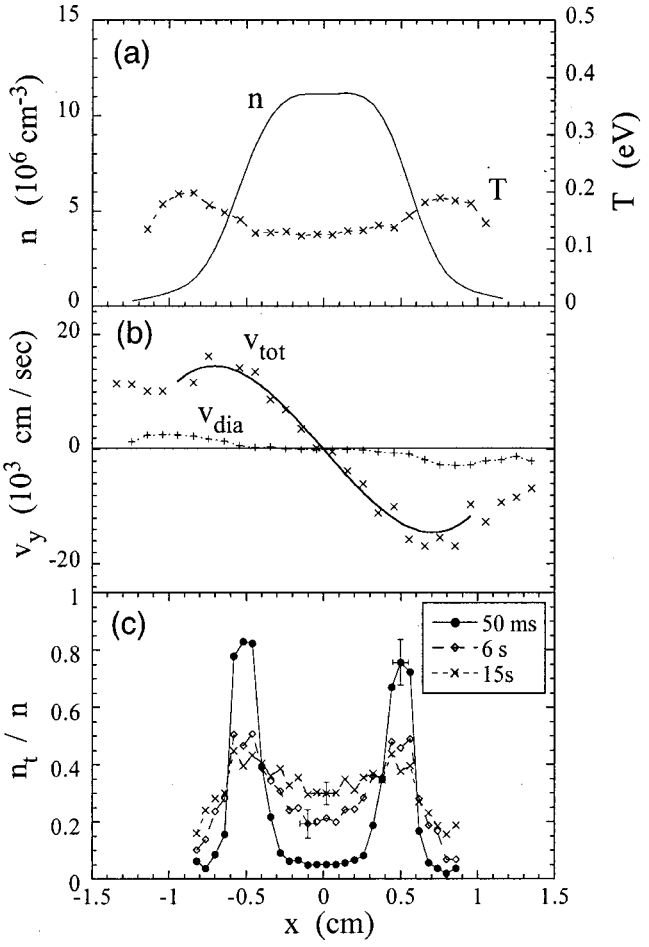

FIG. 3. (a) Density n and temperature T profiles of the quiescent, steady-state ion plasma. (b) Measured fluid rotation velocity $v_{\rm tot}$; and $v_{\rm dia}$ calculated from n and T. (c) Measured test particle concentration n_t/n profiles at three times, showing diffusion of particles.

temperature can be increased by various wave heating techniques, and can be decreased by laser cooling.

This rotating column of ions is maintained in steady state by applying a weak "rotating wall" voltage perturbation which couples angular momentum into the plasma.[19] This counterbalances the weak drag on the column from coupling to the stationary background gas (H_2) and to the stationary θ asymmetries in the magnetic or electric trapping fields. When the same ions are held for days at these pressures, some of the Mg^+ converts to MgH^+, which is not diagnosed by the LIF; but this has little effect on the data presented here.

Figure 3(b) shows the measured total rotation velocity $v_{\rm tot}(r)$, the diamagnetic rotation velocity $v_{\rm dia}(r)$ calculated from $n(r)$ and $T(r)$, and the $\mathbf{E}\times\mathbf{B}$ rotation velocity calculated as $v_{\mathbf{E}}(r) = v_{\rm tot}(r) - v_{\rm dia}(r)$. The individual particles rotate at a rate $\omega_E(r) \equiv v_E(r)/r$, and the shear in this rotation is defined as

$$S(r) \equiv r\frac{\partial}{\partial r}\omega_E(r) \equiv r\omega_E'(r). \tag{1}$$

Note that two particles separated radially by a distance ρ will become separated azimuthally by a distance ρ in a time S^{-1}. The dimensionless scaled shear s is then defined as

$$s(r) \equiv \frac{r\omega_E'}{2\pi ceBn(r)} \sim r\omega_E'/\omega_E, \tag{2}$$

where the last approximation is only valid when the rotation results from near-uniform $n(r)$.

Experimentally, the magnitude of the rotational shear can be controlled by varying the ion density and temperature, or by adjusting the character of the torques and drags on the column. This shear in the θ rotation has only a weak effect on diffusion due to long-range collisions in the 3D regime; but it is the controlling parameter in defining the 2D regime. Indeed, the kinematics of long-range collisions in the presence of shear is parametrized by

$$N_b \equiv \frac{f_b}{S} = \frac{\overline{v}/2L_p}{r\omega_E'}, \tag{3}$$

which is the number of axial bounces executed by a thermal particle before shear separates it in θ from its neighbors.

Figure 3(c) shows an example of the radial diffusion of tagged ions within this steady-state plasma. At $t = 0$, about 80% of the ions at $r = 0.5$ cm are tagged by spin alignment, and the measurement of tagged particle fraction n_t/n at $t = 50$ ms shows good radial localization. After 6 s, substantial transport to $r = 0$ has occurred; and by $t = 15$ s the trapped fraction n_t/n is almost uniform.

The test particle flux is obtained from these measurements as

$$\Gamma_t(r,t) \equiv -\frac{1}{r}\int_0^r dx\, x\frac{\partial}{\partial t}n_t(x,t), \tag{4}$$

with small corrections to the measured n_t to correct for slow spontaneous spin flips. Transport from a local diffusion coefficient $D(r)$ would be expected to give a flux

$$\Gamma_t(r,t) = -D(r)n(r)\frac{\partial}{\partial r}\frac{n_t(r,t)}{n(r)}. \tag{5}$$

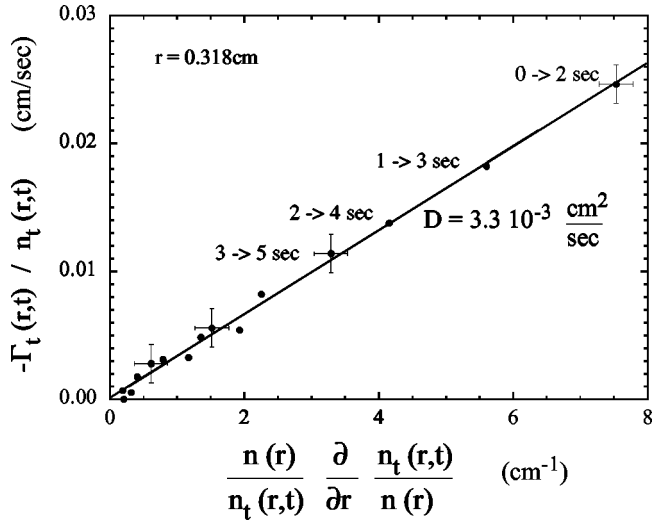

FIG. 4. Measured normalized test particle flux Γ_t/n_t vs normalized test particle density gradient, for several times at one radius. The line represents the Fick's law diffusion of Eq. (5).

This is just Fick's law for test particles, i.e., a diffusive flux proportional to the concentration gradient.

Figure 4 shows the measured normalized flux Γ_t/n_t versus the normalized gradient in the density of test particles, for one radial position. At early times there is a large gradient and a large flux; and the flux decreases at later times as the profile smoothes. The straight line fit illustrates Fick's law with $D=3.3\times10^{-3}$ cm^2/s.

Figure 5 shows the measured diffusion coefficients D obtained for densities $0.1<n<4\times10^7$ cm^{-3}, temperatures $0.05<T<3$ eV, and magnetic fields $0.8<B<4$ T. The diffusion coefficients are normalized by $nB^{-2}\ln(\lambda_D/r_c)$ for comparison to the classical and long-range collision theories; the

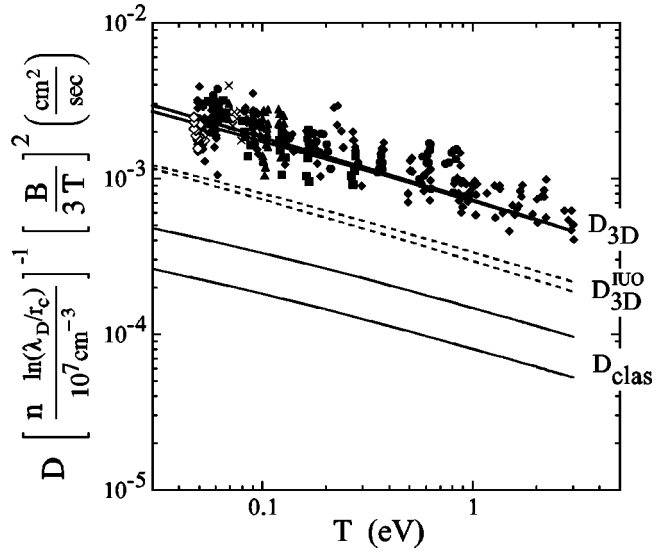

FIG. 5. Measured normalized test particle diffusion coefficients D vs temperature T. Theory curves show classical diffusion $D_{\rm clas}$, long-range diffusion $D_{3D}^{\rm IUO}$ calculated by integration along unperturbed orbits, and a proper calculation of D_{3D} including "velocity caging."

un-normalized diffusion coefficients varied by a factor of 25 as B was varied, and by a factor of 40 as n was varied.

Over a wide range of temperatures, the measured diffusion is about ten times larger than predicted for classical collisions, due to long-range $\mathbf{E}\times\mathbf{B}$ drift collisions between ions. The initial analysis of diffusion from long-range collisions[6] used the standard theory technique of integration along unperturbed orbits (IUO), and gave a prediction $D_{\rm IUO}$ about $3\times$ larger than classical but about $3\times$ smaller than the measurements. A more thorough analysis[7] revealed a new "velocity-caging" effect which occurs in one-dimensional collisions, and the revised prediction D_{3D} agrees closely with the measurements.

The diffusion due to these long-range $\mathbf{E}\times\mathbf{B}$ drift collisions can be estimated rather simply.[20] Two guiding centers separated by a distance of λ_D have an interaction electric field of e/λ_D^2, and take a cross-field $\mathbf{E}\times\mathbf{B}$ drift step of order $\Delta t(c/B)(e/\lambda_D^2)$, where $\Delta t\sim\lambda_D/\overline{v}$ is the time for the collision. This step is very small compared to r_c. However, the frequency of such collisions is of order $n\overline{v}\lambda_D^2$, which is large compared to the Coulomb collision frequency $\nu_c=n\overline{v}b^2$, where $b\equiv e^2/T$ is the classical distance of closest approach. The diffusion is then given by

$$D\sim n\overline{v}\lambda_D^2[\Delta tce/(B\lambda_D^2)]^2=\nu_c r_c^2. \tag{6}$$

This was first estimated by Lifshitz and Pitaevskii.[5]

A detailed calculation[8,7] of the diffusion from these 3D long-range collisions yields

$$D_{3D}^{(\rm IUO)}=2\sqrt{\pi}\,n\overline{v}b^2r_c^2\ln\left(\frac{\overline{v}}{\Delta v_{\min}}\right)\ln\left(\frac{\lambda_D}{r_c}\right). \tag{7}$$

The superscript (IUO) indicates that the technique of integration along unperturbed orbits was used. The logarithmic divergence with λ_D/r_c is due to the large $\mathbf{E}\times\mathbf{B}$ drifts that arise when guiding centers undergo a close approach; the cutoff at r_c reflects the fact that the guiding center theory for the dynamics breaks down for impact parameters $\rho<r_c$. The velocity $\Delta v_{\min}$ is the minimum relative velocity Δv between two interacting particles for which the unperturbed orbit analysis is still valid; particles with small Δv_z experience the largest drifts.

The lower limit $\Delta v_{\min}$ will be set either by shear in the plasma rotation or by velocity-scattering collisions with other particles. The latter mechanism dominates in our experiments, giving $\Delta v_{\min}\approx(\mathcal{D}_v/\sqrt{r_c\lambda_D})^{1/3}$, where $\mathcal{D}_v\approx n\overline{v}^3b^2$ is the *velocity-space* diffusion coefficient.

The IUO technique presumes that two particles interact only once as they pass by one another along the magnetic field. However, velocity scattering collisions with surrounding particles eventually cause the relative axial velocity of the interacting pair to reverse, and the particles may have another collision; surprisingly, they effectively collide three times. In essence, collisions cause velocity "caging" of particles with $\Delta v_z\gtrsim\Delta v_{\min}$, causing them to interact more strongly than they would otherwise. The result of this effect is an increase in the diffusion coefficient by a factor of $\alpha=3$, giving

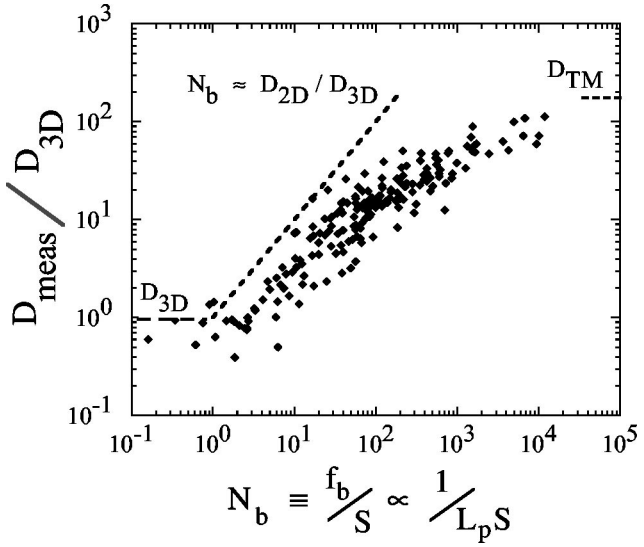

FIG. 6. Measured diffusion D_{meas} normalized by the 3D prediction D_{3D} vs number of particle bounces N_b, showing enhanced diffusion in the 2D bounce-average regime.

$$D_{3D} = 2\alpha\sqrt{\pi}\, n\bar{v} b^2 r_c^2 \ln\left(\frac{\bar{v}}{\Delta v_{\min}}\right)\ln\left(\frac{\lambda_D}{r_c}\right) \tag{8}$$

with $\alpha = 3$.

The enhancement by α is denoted separately because very large shear in the background flow could eliminate the caging effect and give $\alpha \approx 1$. This occurs because particles are sheared apart in θ before they have time to reverse their velocities and collide again. Overall, Eq. (8) is in quantitative agreement with the diffusion measurements, as shown by the solid line in Fig. 5.

III. BOUNCE ENHANCEMENT OF DIFFUSION

Enhancement of the test particle diffusion above D_{3D} of Eq. (8) is observed in regimes where $N_b \gg 1$. Ions move rather slowly, and the data of Sec. II were in the 3D regime of $N_b < 2$. Larger values of N_b can be obtained by decreasing the axial length of the column ($0.7 < L_p < 10$ cm); and by considering radii where the scaled shear s is small ($10^{-4} < s < 0.1$).

Figure 6 shows the measured diffusion coefficient enhancement D/D_{3D} vs N_b. For $N_b < 1$, the solid line represents D_{3D}, and the data points would overlay those of Fig. 5. For $N_b > 1$, the diffusion increases proportional to N_b, approaching the shear-free Taylor–McNamara limit discussed in the following. The solid line represents $D_{2D}/D_{3D} = N_b$, also derived in the following.

We note that the parameters of this bounce enhancement are not consistent with the 3D perspective. The theory of 3D collisions focuses on pairs of particles with small *relative* velocity Δv_z, so the thermal velocity $\bar{v}$ and the plasma length L_p should not enter; effects from end confinement fields have been analyzed with regard to viscosity in finite length systems.[15] Apparently, the enhancement represents an increase in the diffusion from 2D collision kinetics.

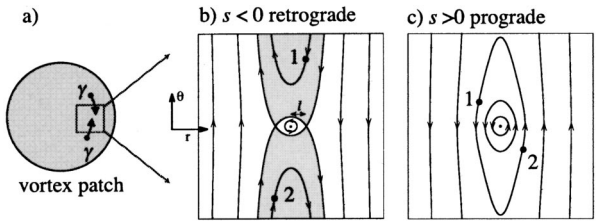

FIG. 7. (a) Collisional interaction of two point vortices in a vortex patch with shear, (b) streamlines in the rotating frame for the interaction region for negative shear, giving retrograde vortices, and (c) positive shear, giving prograde vortices.

A. 2D diffusion with shear

This enhanced diffusion is now understood as resulting from the bounce-averaged (or $k_z = 0$) component of the long-range collisions, since this 2D diffusion increases with decreasing background shear.[14,21] Furthermore, this perspective of shear reduction of 2D transport connects well with the early theoretical work on 2D diffusion due to macroscopic fluctuations in shear-free plasmas.[22,23]

From the 2D perspective, each ion is a z-average "rod" of charge which $\mathbf{E}\times\mathbf{B}$ drifts in (r,θ) due to the fields of all the other ions. The $\mathbf{E}\times\mathbf{B}$ drift dynamics of a collection of N charged rods is isomorphic to a 2D gas of N point vortices: each rod, with charge $\bar{q} \equiv e/L_p$ per unit length, is equivalent to a point vortex with circulation

$$\gamma \equiv \bar{q}(4\pi c/B) = 4\pi c e B/L_p. \tag{9}$$

(Here, we take $\gamma > 0$ and $\omega_E > 0$ for positive ions by choosing $\mathbf{B} = -B\hat{z}$; for electrons, choosing $B = +B\hat{z}$ would similarly give $\gamma > 0$.)

Early work on diffusion of 2D point vortices focused on the case of a quiescent, homogeneous shear-free gas.[22,23] When the vortices are distributed randomly, representing high-temperature thermal fluctuations, Taylor and McNamara showed that the diffusion coefficient (for diffusion in one direction) has the following simple form:

$$D_{TM} = \frac{\gamma}{8\pi}\sqrt{N}. \tag{10}$$

The diffusion coefficient is not an intensive quantity, because the diffusion process is dominated by large "Dawson–Okuda vortices" whose size is of order the system size.[23] However, for finite temperature, these authors all suggested that Debye shielding limits the maximal vortex size to approximately the Debye length λ_D.

Here, we show that in the presence of applied shear, the Dawson–Okuda vortices are disrupted and the diffusive transport is greatly reduced[14,21] compared to Eq. (10). This result may be relevant to current experiments and theories in fusion plasmas, which also observe reduced transport in the presence of shear.[18] In such plasmas, the fluctuations are unstable and turbulent; and so the transport is difficult to determine theoretically. However, in a stable gas of point vortices, the statistical theory described here determines the transport explicitly.

The theory analyzes collisions in a circular patch of vortices with uniform 2D areal density $\bar{n} \equiv N/\pi R_p^2$, as shown

in Fig. 7. To this vortex patch an *external* sheared rotation $\omega(r)$ is applied, with uniform shear rate $S \equiv r\omega'$ and scaled shear $s = S/\bar{n}\gamma$. In physical systems, the rotation $\omega(r)$ would follow from $\bar{n}(r)$ through Poisson's equation, and a uniform patch would have $\omega = \bar{n}\gamma/2$.

The character of vortex collisions, diffusion, and dynamics depends critically on whether the shear is negative or positive, i.e., whether the vortices are retrograde or prograde. (A retrograde vortex rotates in the *opposite* sense compared to the local curl of the sheared flow.) Indeed, the theory will be seen to be valid only for $s<0$ (retrograde vortices). Fortunately, this corresponds to the experiments, which have monotonically decreasing $\omega(r)$; each ion is a retrograde vortex in the negative overall shear flow.

For $s<0$, two separate collisional processes are responsible for radial diffusion in the presence of applied shear: small impact parameter collisions, described by a Boltzmann formalism; and large impact parameter collisions, described by a quasilinear formalism. In Fig. 7(b), the shaded region shows the range of possible streamlines (in the rotating center-of-mass frame) for small impact parameter collisions. For example, vortex 1 may flow down (in θ) and to the left (in r) and then back up because of a collision with vortex 2, which correspondingly flows up, to the right, and back down. The unshaded region shows possible large impact parameter collisions, where the vortices would merely move in and back out slightly while streaming past each other, except for the influence of other distant vortices.

Here small and large impact parameters mean initial radial separations that are smaller or larger than a distance $2l$, where the "trapping distance" l is defined as

$$l \equiv \sqrt{-\gamma/4\pi S} = a/\sqrt{-2s}. \tag{11}$$

Here, $a \equiv (\pi\bar{n})^{-1/2}$ is the average distance between vortices. Note that the trapping distance is undefined for $s>0$, since the trapping extends to infinity in this simple model.

An estimate of the vortex diffusion is obtained by considering small impact collisions. Here, the radial step size is $\Delta r \sim l$, and the collision rate is the rate at which the shear brings vortices together, i.e., $\nu \sim \bar{n}|S|l^2$. This gives a diffusion $D = \nu \Delta r^2 \propto \bar{n}|S|l^4 \propto \gamma s^{-1}$.

A rigorous Boltzmann calculation gives the radial diffusion coefficient D_B due to these small impact parameter collisions; and a quasilinear calculation based on the Kubo formula gives the diffusion coefficient D_K from multiple distant collisions. The total diffusion[14] is then

$$D_{2D} = D_B + D_K = \frac{\gamma}{2s}\frac{1}{\pi^2}\ln^2 \Lambda_B + \frac{\gamma}{2s}\ln(r/\rho_{\min})$$

$$= \frac{2\pi ec}{L_p B s}\left[\frac{\ln^2 \Lambda_B}{\pi^2} + \ln(r/\rho_{\min})\right], \tag{12}$$

with collision logarithms given by $\Lambda_B \equiv 2.713\pi^2 S^2/\bar{n}\gamma^2$ and $\rho_{\min} \approx (4D_K/S)^{1/2}$ for the regimes of interest here.

Of course, this estimate is valid only when it is less than the zero-shear result, i.e., when $D_{2D} < D_{TM}$. However, one can see that even a very small shear, of order $S/\bar{n}\gamma \approx N^{-1/2}$, is required to make the zero-shear D_{TM} inapplicable. In other words, even small shears wipe out the large-scale Dawson–Okuda vortices required to give D_{TM}.

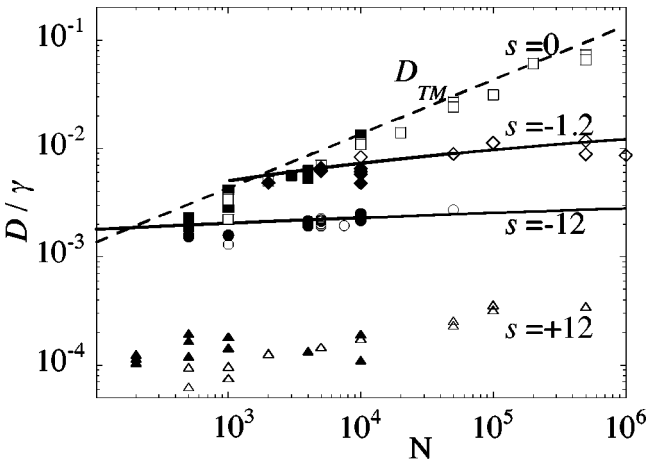

FIG. 8. Diffusion coefficients D from simulations vs number of particles N, for shear rates $s=0$, -1.2, -12, and 12. Solid points are MD simulations; open points are PIC simulations. The dashed line is Eq. (10); the solid lines are Eq. (12). No theory predicts the weaker diffusion for positive shear (prograde vortices).

We have tested this theory using numerical simulations[14] of N identical point vortices, initially placed randomly inside a circular patch, with an applied uniform external shear rate S. As a check of the numerics, we employed two separate simulation techniques, a 2D molecular dynamics (MD) method for point vortices, and a 2D particle in cell (PIC) simulation. To obtain the diffusion coefficient, we chose as test particles all vortices in the band of radii from $0.43R$ to $0.57R$, and followed their mean square change in radial position, $\langle \delta r^2(t) \rangle$. The diffusion coefficient is found from fitting $\langle \delta r^2(t) \rangle = 2Dt$.

Figure 8 displays the diffusion rates obtained from the simulations with varying N compared to the predictions of theory. The simulations with $s=0$ agree closely with D_{TM} (dashed line). Simulations with negative imposed shears of $s=-1.2$ and -12 show reduced diffusion, in quantitative agreement with D_{2D} (solid lines).

However, the simulations with $s=+12$ show about $10\times$ less diffusion, apparently due to trapping effects in collisions between vortices which are prograde with respect to the shear. In essence, the trapping size l is infinite for $s>0$, and the effects of bound vortex pairs cannot be ignored; thus, the Boltzmann analysis is inapplicable. Furthermore, the method of integration along unperturbed orbits, which is essential to the Kubo analysis, also fails. Analysis of these trapped particle effects is a significant unsolved theory problem.

We note further that these same trapping effects cause a decreased velocity for *macroscopic* prograde vortices moving up or down a background vorticity gradient.[24] The trapping is a critical aspect of the microscopic collisions and of the macroscopic dynamics.

For perspective, we note that both the Taylor–McNamara diffusion and the collisional diffusion follow from the discreteness of the vorticity. If we let the discreteness go to zero by letting $N \to \infty$ at *fixed total circulation*, or

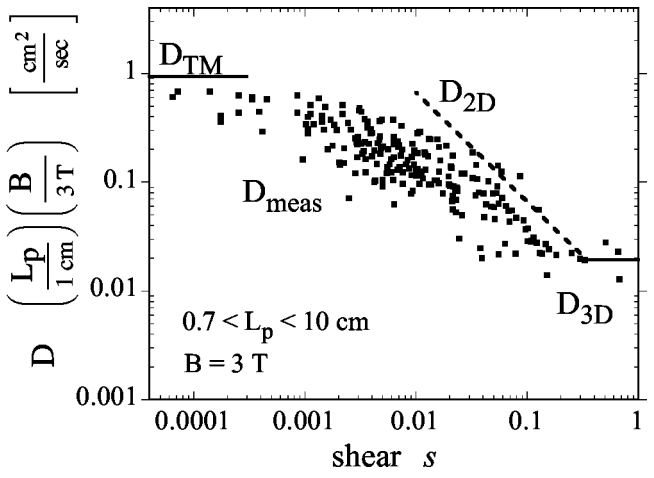

FIG. 9. Measured diffusion vs measured shear s, showing shear-reduction of diffusion from the zero-shear Taylor–McNamara limit to the 3D regime. In the 2D regime, the diffusion scales as L_p^{-1} and B^{-1}.

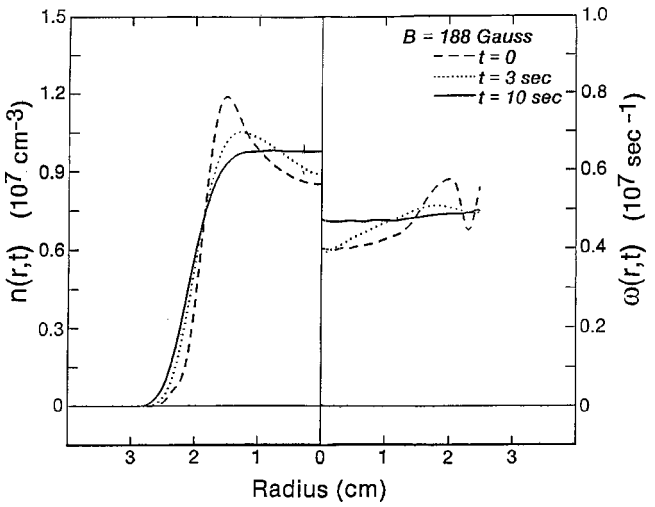

FIG. 10. Measured electron density profiles $n(r,t)$ and total rotation profiles $\omega_R(r,t)$ at three different times t, showing viscous relaxation to the rigid-rotor thermal equilibrium.

equivalently look at the normalized $D/N\gamma$, then the diffusion will *decrease* as N increases. From the perspective of Fig. 8, the shear-free diffusion $D_{\rm TM}/N\gamma$ decreases as $N^{1/2}$, since the fluctuation-induced Taylor–McNamara vortices are weaker. On the other hand, for finite scaled shear s, the scaled diffusion $D/N\gamma$ decreases as N^{-1} since the collisionality is proportional to the discreteness.

Returning to the ion experiments, this perspective of shear reduction of 2D diffusion provides a complete explanation of the length-dependent diffusion enhancements, since the experiments are only in the negative shear regime where the theory applies. Figure 9 displays the same experimental data as Fig. 6, but with the diffusion scaled as DL_pB and plotted versus scaled shear s. The diffusion approaches $D_{\rm TM}$ for $|s|<10^{-3}$, decreases as $|s|^{-1}$ for $10^{-2}<|s|<10^{-1}$, and equals D_{3D} for $|s|>1$. Here, the column lengths ranged over $0.7<L_p<10$ cm, and the temperature ranged over $0.05<T<3$ eV, with fixed $B=3T$. The temperature and shear were closely related, since the near-equilibrium plasmas have near-uniform $\omega_{\rm tot}$, so the shear in ω_E arises mainly from the diamagnetic drift as $T\nabla n$. The estimate $D_{\rm TM}$ is from the $N=5\times10^7$ ions within the low-shear region of the plasma. The estimate D_{3D} uses T and n, as is characteristic of the data points on Fig. 9 with large shear.

Considering the plasma parameters one at a time helps clarify the relation between the 3D and 2D regimes of long-range collisions. Figure 5 shows $D\propto T^{-1/2}$, but presumably this would show $D\propto T^0$ at high temperatures if the shear were held fixed. The transition to this 2D regime would occur when the 3D $\Delta v_z\approx0$ resonance gave negligibly small diffusion. From this perspective, the diffusion "enhancement" of Fig. 6 with increasing temperature (increasing f_b) appears only because D_{3D} decreases as $D_{3D}\propto T^{-1/2}$.

The length dependence of the diffusion in the 2D regime is somewhat surprising, but consistent with the 2D analysis. Consider increasing the length of the plasma column by appending M identical sections with identical $n(r)$ and $\omega_E'(r)$. The diffusion will then *decrease* because the $k_z=0$ strength $\gamma\propto e/L_p$ of each electron decreases by M, while $\overline{n}\gamma$ and s remain constant; this is essentially taking the "plasma limit" of zero discreteness.

B. Viscosity and heat conduction

Long-range collisions also transfer angular momentum and energy, giving viscosity[15,16] and heat conduction[12,13] coefficients which may be substantially larger than the classical coefficients. The long-range viscosity is especially striking in pure electron plasmas, being up to 10^8 times larger than classical, with a dependence on L_p and N_b which is not yet fully understood.[16] Long-range heat transport measured in pure ion plasmas in the 3D regime is up to 10^3 times classical.[13] Theory suggests there is no 2D enhancement of heat transport, but this has not been checked experimentally.

Viscosity acting on a sheared rotating plasma causes a bulk transport of particles, with a consequent relaxation toward a uniform profile of total fluid rotation $\omega_{\rm tot}$. Figure 10 shows measurements of this relaxation in a pure electron plasma.[10] The density profile $n(r,z=0)$ relaxes toward the thermal equilibrium profile, which is uniform in the center and then falls off on a scale of λ_D. Here, the z dependence of the density $n(r,z)$ is obtained from the measured z-integrated density $Q(r)=\int dz\, n(r,z)$ using an $(r-z)$ Poisson solver which presumes local equilibrium along each field line. In this evolution, the total angular momentum is well conserved, as some electrons move out and others move in, verifying that the transport is indeed due to "internal" electron–electron collisions.

Figure 10 also shows the calculated rotation profiles relaxing toward a rigid rotor with $\omega_{\rm tot}(r)=$constant. Here, the Poisson solution gives $E(r,z)$ and $\omega_E(r,z)=cE/rB$; the diamagnetic rotation $\omega_{\rm dia}(r,z)=c\nabla(nT)/enrB$ is calculated from the density and measurements of temperature $T(r)$; and the total fluid rotation is calculated as $\omega_{\rm tot}=\omega_E+\omega_{\rm dia}$.

Local kinematic viscosity coefficients η are obtained[16] from these evolutions, by fitting the data to a fluid model of the z-averaged particle flux $\overline{\Gamma}(r,t)$. The measured flux is

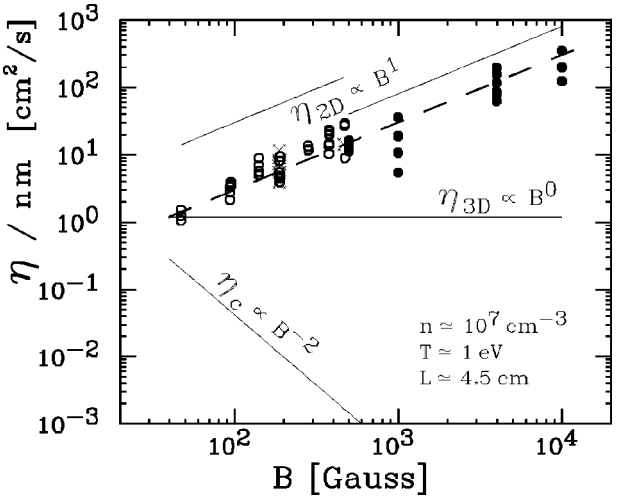

FIG. 11. Measured electron viscosity η vs magnetic field B, compared to the classical, 3D, and 2D predictions of Eqs. (15), (16), and (17).

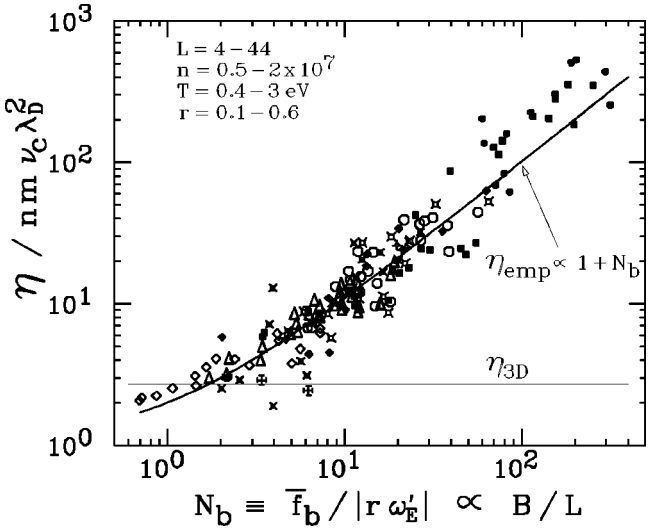

FIG. 12. Measured electron viscosity η vs the effective number of bounces N_b, compared to η_{3D} of Eq. (16) and to the empirical scaling η_{emp} of Eq. (18).

$$\Gamma(r,t) \equiv -\frac{1}{L_p r}\int_0^r dr'\, r' \frac{d}{dt} Q(r,t), \tag{13}$$

and this flux is driven by viscosity η acting on shears in ω_{tot}, as

$$\Gamma(r,t) \equiv n v_r = -\frac{c}{eB}\frac{1}{r^2}\frac{\partial}{\partial r} r^2 \eta r \frac{\partial}{\partial r}\omega_{tot}. \tag{14}$$

The viscosity coefficient η is relatively well determined at radii where the shear and flux are large.

The classical theory of short-range velocity-scattering collisions[1–3] gives

$$\frac{\eta_c}{nm} = \frac{2\sqrt{\pi}}{5} n \bar{v} b^2 r_c^2 \ln\left(\frac{r_c}{b}\right) \propto B^{-2} L_p^0. \tag{15}$$

Long-range $\mathbf{E}\times\mathbf{B}$ drift collisions in the 3D regime are predicted[6,7,9] to give

$$\frac{\eta_{3D}}{nm} = \alpha \frac{\sqrt{\pi}}{3} n \bar{v} b^2 \lambda_D^2 \ln\left(\frac{\bar{v}}{\Delta v_{min}}\right) \propto B^0 L^0, \tag{16}$$

where the velocity-caging factor α and minimum relative velocity Δv_{min} have the same meaning as in Eq. (8). The recent 2D bounce-averaged theory[15] incorporates an approximation to the drifts from thermal electron penetration into the end sheaths, and predicts transport driven by shears in ω_{tot} (but limited by shears in ω_E) as

$$\frac{\eta_{2D}}{nm} = 16\pi^2 n \bar{v} b^2 d^2 N_b g\left(\frac{2d}{r}\right) \propto B^2 L^{-3}, \tag{17}$$

with $d \equiv \bar{v} r_c |L'/L| S^{-1} = 2 r_c L' N_b$ being the predicted radial interaction distance, and $g(2d/r) \approx 0.1$ being a collision integral.

Figure 11 shows the measured viscosity coefficient η versus magnetic field B for relatively short plasmas ($L_p \approx 5$ cm, $T \approx 1$ eV) compared to the three theory estimates. The viscosity coefficient scales as $\eta \propto B^1$ over two decades in B; for $B = 10$ kG, the measured η is 10^8 times larger than the η_c predicted for short-range velocity-scattering collisions. The data scale with B as does η_{2D}, but the data is $3-10\times$ smaller for these short plasmas.

The measured viscosity depends strongly on plasma length L_p, although not as predicted by η_{2D}. Empirically, we find that the parameter N_b alone characterizes both the B and L dependence rather accurately; all of the data are well described[16] by

$$\frac{\eta_{emp}}{nm} = (1 + N_b) n \bar{v} b^2 \lambda_D^2 \propto B^1 L^{-1}. \tag{18}$$

Figure 12 shows the measured viscosity for a wide range of n, L, T, and B. For long plasmas and/or low magnetic fields, with $N_b \lesssim 1$, the measured data shows factor-of-2 agreement with the 3D infinite-length theory. In this regime, the radial shears apparently separate the interacting particles and prevent multiple correlated collisions. For short plasmas and/or high fields, with $N_b \gg 1$, the measured viscosity is enhanced by an amount that is observed to scale as N_b, most probably due to multiple correlated collisions.

The 2D viscosity theory treats the ''resonant'' interaction between two rods at different radii; that is, the rods interact for a long time if $\omega_1(r_1) = \omega_2(r_2)$. An early analysis[9] considered only nonmonotonic rotation frequencies $\omega_E(r)$ (like Fig. 10), so that the resonance was satisfied at distinct radii where $\omega_E(r_1) = \omega_E(r_2)$. Moreover, the plasma temperature did not enter the early 2D analysis, suggesting that the viscous transport was driven by shears in ω_E, and that this transport would cease when $\omega_E(r) =$ constant rather than when $\omega_{tot}(r) =$ constant. Experiments have demonstrated[16] that the 2D viscosity enhancements are essentially the same for monotonic and nonmonotonic profiles, and that the viscous transport is driven by shears in $\omega_{tot}(r)$ rather than by shears in $\omega_E(r)$.

The recent 2D viscosity analysis[15] includes the temperature T and length L_p of the plasma by including an approximation to the θ drifts[25] which occur due to the end confine-

ment fields. A particle reflecting off the end receives an axial impulse $2mv_z$ and drifts in $\hat{\theta}$ by an amount proportional to $2mv_z$. The particle's bounce-averaged $\mathbf{E}\times\mathbf{B}$ drift rotation frequency $\langle\omega_E\rangle_z$ then depends on v_z, and the transport resonance can be satisfied if $\langle\omega_E(r_1,v_{z1})\rangle_z=\langle\omega_E(r_2,v_{z2})\rangle_z$. This analysis gives η_{2D} of Eq. (17), which is in qualitative agreement with the experiments. However, the measured viscosity is about $3\times$ smaller than predicted by Eq. (17), and does not show the shear and length dependencies appearing in the predicted radial interaction distance d.

Thus, the empirical 2D viscosity enhancement by a factor of N_b is intriguingly similar to the 2D diffusion enhancement by a factor of N_b; but the viscosity enhancement is not yet supported by theory.

Finally, we mention heat transport coefficients, to complete the picture presented by Table I. The cross-field energy flux is driven by temperature gradients, as $\Gamma_{\mathcal{E}}=-\kappa\partial T/\partial r$, with the coefficient of heat conduction κ related to the thermal diffusivity χ by $\kappa=(5/2)n\chi$.

In classical velocity-scattering collisions[4] with $b<\rho<r_c$, the particles step a distance r_c and carry their thermal energy with them, giving $\chi\propto\nu_c r_c^2$ or

$$\frac{2}{5n}\kappa_{\mathrm{clas}}=\frac{16\sqrt{\pi}}{15}\nu_c r_c^2\ln(r_c/b)\propto nT^{-1/2}B^{-2}. \tag{19}$$

For long-range collisions in the 3D (not bounce-averaged) regime, with impact parameters $r_c<\rho<\lambda_D$, the collisions are effectively one-dimensional and elastic, and the particles merely exchange axial velocities. A rigorous analysis[12] of these collisions gives

$$\frac{2}{5n}\kappa_{3D}=(0.48)\nu_c\lambda_D^2\propto T^{-1/2}. \tag{20}$$

Note that this thermal diffusivity is *independent* of magnetic field B and of plasma density n.

Figure 13 shows that measurements[13] in pure ion plasmas give quantitative agreement with Eq. (20) over a wide range of temperatures, densities, and magnetic fields. At low densities and high magnetic fields, classical collisions give very low thermal diffusivity, and long-range heat transport is up to $10^3\times$ larger. At low temperatures, classical collisions are further suppressed as the cyclotron radius r_c decreases toward the distance of closest approach b; the visible bend in the theory curves of Fig. 13 is from $\ln(r_c/b)$. Indeed, at very low temperatures where $r_c<b$, the perpendicular-to-parallel thermal isotropization is suppressed completely,[26] yet the long-range heat transport remains large.

Theory suggests that there is no 2D enhancement to the heat transport, since 2D rods have no axial velocity to exchange. The heat transport experiments of Ref. 19 were all performed in the 3D regime: even for the highest temperatures, one has $N_b<1$, since the column was long and the shear was large. The question of heat transport among rapidly bouncing particles thus remains open.

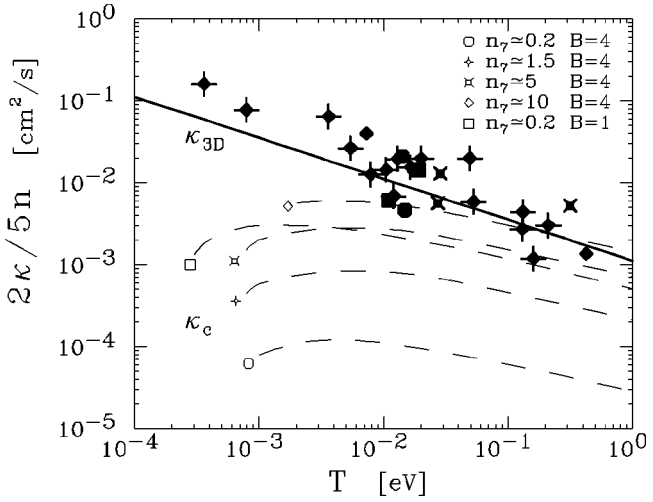

FIG. 13. Measured thermal diffusivity $2\kappa/5n$ vs temperature T. Solid line shows Eq. (20) for long-range collisions, which is independent of density and magnetic field; dashed lines show classical predictions of Eq. (19) for the n and B of the experiments.

More significantly, the possibility of thermal wave emission and absorption contributing to "very long range" transport of energy was first analyzed by Rosenbluth and Liu.[11] Later analysis suggests that both thermal conduction and viscosity may be dominated by wave transport for large plasma radii R_p.[12,20] For heat transport, wave transport is expected to dominate when $R_p\gtrsim10^2\lambda_D$; and for viscosity, $R_p\gtrsim10^3\lambda_D$ is required. Future experiments with cold ion plasmas[27] may characterize this wave-mediated transport.

ACKNOWLEDGMENTS

This work is supported by Office of Naval Research Grant No. ONR N00014-96-1-0239 and National Science Foundation Grant No. PHY-9876999.

[1] C. L. Longmire and M. N. Rosenbluth, Phys. Rev. **103**, 507 (1956).
[2] A. Simon, Phys. Rev. **100**, 1557 (1955).
[3] T. M. O'Neil and C. F. Driscoll, Phys. Fluids **22**, 266 (1979).
[4] M. N. Rosenbluth and A. N. Kaufman, Phys. Rev. **109**, 1 (1958).
[5] E. M. Lifshitz and L. P. Pitaevskii, *Physical Kinetics* (Pergamon, New York, 1981), p. 273.
[6] T. M. O'Neil, Phys. Rev. Lett. **55**, 943 (1985).
[7] D. H. E. Dubin, Phys. Rev. Lett. **79**, 2678 (1997).
[8] F. Anderegg, X.-P. Huang, C. F. Driscoll, E. M. Hollmann, T. M. O'Neil, and D. H. E. Dubin, Phys. Rev. Lett. **78**, 2128 (1997).
[9] D. H. E. Dubin and T. M. O'Neil, Phys. Rev. Lett. **60**, 1286 (1988).
[10] C. F. Driscoll, J. H. Malmberg, and K. S. Fine, Phys. Rev. Lett. **60**, 1290 (1988).
[11] M. N. Rosenbluth and C. S. Liu, Phys. Fluids **19**, 815 (1976).
[12] D. H. E. Dubin and T. M. O'Neil, Phys. Rev. Lett. **78**, 3868 (1997).
[13] E. M. Hollmann, F. Anderegg, and C. F. Driscoll, Phys. Rev. Lett. **82**, 4839 (1999); Phys. Plasmas **7**, 1767 (2000).
[14] D. H. E. Dubin and D.-Z. Jin, Phys. Lett. A **284**, 112 (2001).
[15] D. H. E. Dubin and T. M. O'Neil, Phys. Plasmas **5**, 1305 (1998).
[16] J. M. Kriesel and C. F. Driscoll, Phys. Rev. Lett. **87**, 135003 (2001).
[17] A. A. Ware, Phys. Fluids B **5**, 2769 (1993).
[18] K. H. Burrell, Phys. Plasmas **4**, 1499 (1997); P. W. Terry, Rev. Mod. Phys. **72**, 109 (2000); H. Biglari, P. H. Diamond, and P. W. Terry, Phys. Fluids B **2**, 1 (1990).

[19]E. M. Hollmann, F. Anderegg, and C. F. Driscoll, Phys. Plasmas **7**, 2776 (2000).
[20]D. H. E. Dubin, Phys. Plasmas **5**, 1688 (1998).
[21]D. H. E. Dubin and D. Z. Jin, in *Non-Neutral Plasma Physics III* [AIP Conf. Proc. **498**, 233 (1999)].
[22]J. B. Taylor and B. McNamara, Phys. Fluids **14**, 1492 (1971).
[23]J. M. Dawson, H. Okuda, and R. N. Carlile, Phys. Rev. Lett. **27**, 491 (1971); H. Okuda and J. M. Dawson, Phys. Fluids **16**, 408 (1973).
[24]D. A. Schecter and D. H. E. Dubin, Phys. Rev. Lett. **83**, 2191 (1999).
[25]A. J. Peurrung and J. Fajans, Phys. Fluids B **5**, 4295 (1993).
[26]B. R. Beck, J. Fajans, and J. H. Malmberg, Phys. Rev. Lett. **68**, 317 (1992); Phys. Plasmas **3**, 1250 (1996).
[27]F. Anderegg, C. F. Driscoll, and D. H. E. Dubin, in *Non-Neutral Plasma Physics IV* [AIP Conf. Proc. **606,** 401 (2002)].